High-throughput screening for antiferromagnetic Heusler compounds using density functional theory

Jan Balluff,* Kevin Diekmann, Günter Reiss, and Markus Meinert†
Center for Spinelectronic Materials and Devices, Bielefeld University, D-33501 Bielefeld, Germany
(Received 6 April 2017; revised manuscript received 2 June 2017; published 14 August 2017)

Commonly used antiferromagnets contain expensive precious metals, which limits their applicability. Novel materials that are made of abundant elements are thus required for a large scale application, e.g., in spintronic devices. We propose a combinatorial, high-throughput approach based on density functional theory calculations to search for such new antiferromagnets. The power of the method is demonstrated by screening the ternary Heusler compounds for antiferromagnetic phases. We utilize the AFLOWLib, a computational materials database that contains over one million ternary phases. Among these we identify 291 potentially stable magnetic Heusler compounds. By explicitly checking for antiferromagnetic configurations we identify 70 antiferromagnetic Heusler compounds. Comparison with available experimental data shows that the method has excellent selectivity: all known antiferromagnetic Heusler compounds are correctly identified and no material is erroneously assigned an antiferromagnetic ground state. By calculating the Néel temperatures we predict 21 antiferromagnetic Heusler compounds with a Néel temperature above room temperature.

DOI: 10.1103/PhysRevMaterials.1.034404

I. INTRODUCTION

Spintronic devices use the spin of the electrons to manipulate and store information within magnetic materials. Naturally, ferromagnetic materials play a key role in such devices, since their magnetization is easily manipulated with currents or external fields and their magnetization state allows us to encode binary information. Large steps forward in this field followed the discovery of the giant magnetoresistance (GMR) in the late 1980s by Fert and Grünberg [1,2], where a resistance change in a thin film multilayer stack of alternating ferromagnetic and nonmagnetic metals could be observed depending on the relative orientations of the magnetizations. In a similar way, a resistance change can be observed in magnetic tunnel junctions based on the tunneling magnetoresistance (TMR) [3,4]. Here the ferromagnetic layers are separated by a thin insulating barrier. GMR and TMR devices are currently used in almost every hard disk drive read head and fast, nonvolatile, and low-power magnetic memory based on magnetic tunnel junctions is the subject of current research [4,5]. Typically, these devices contain two magnetic layers, one of which is free to follow external fields or to be manipulated by spin-transfer torque [6,7], whereas the second layer is magnetically fixed and serves as the reference for the magnetization state of the free layer. This reference is prepared using the exchange bias effect [8], which occurs in ferromagnet/antiferromagnet bilayers due to the exchange coupling across the interface and the uniaxial anisotropy of the antiferromagnet [9]. Due to the exchange bias, the hysteresis loop of the ferromagnetic film is shifted; if the shift is larger than the coercive field of the material, a single, well-defined magnetic state at zero field is created.

In the recently emerging field of antiferromagnetic spintronics [10], an antiferromagnetic layer is used as the active component, e.g., to store information in its magnetic state. Successful experiments demonstrating electrical switching and magnetic state readout of an antiferromagnet have already been demonstrated in a material with specific symmetries [11].

The most commonly used antiferromagnetic materials for exchange bias applications are IrMn and PtMn due to their good thermal stability and corrosion resistance [12]. Unfortunately, Ir and Pt are among the the least abundant elements on earth [13]. The increasing demand, especially for future mass production of magnetic memory devices, cannot be satisfied by the current Ir and Pt supply, resulting in a huge price increase in recent years. Therefore, a suitable material with similar properties but more abundant constituents is urgently searched for. Although still new binary antiferromagnets with useful properties are discovered occasionally [14], no breakthrough discoveries have been made among binary antiferromagnets in recent years. Thus, the search for novel materials has to be extended to ternary compounds.

Here we investigate the class of Heusler compounds and perform a search for antiferromagnetic ground states among these. These materials have the general chemical formula X_2YZ and crystallize in the $L2_1$ structure (space group $Fm\bar{3}m$, No. 225), an inversion-symmetric fcc structure with a four-atom basis, which is closely related to the zinc blende structure. From a combinatorial point of view, there are hundreds of thousands of possible combinations to form a Heusler compound, making a systematic analysis and search necessary. We utilize the AFLOWLib [15], a computational database for materials with a special focus on the Heusler type structures for ternary compounds. The calculations therein are based on density functional theory (DFT), which allows us to predict many properties such as formation energies or magnetic states. The calculations are done combinatorially, so every possible ternary composition is considered. The results are stored for further processing and can be searched for numerous criteria, which sets the base for our screening. In the first step, a list of possible candidates is extracted from the AFLOWLib based on a database search. In the second step, the phase stability is investigated. For candidates which are stable against phase decomposition, explicit calculations of

*balluff@physik.uni-bielefeld.de
†meinert@physik.uni-bielefeld.de

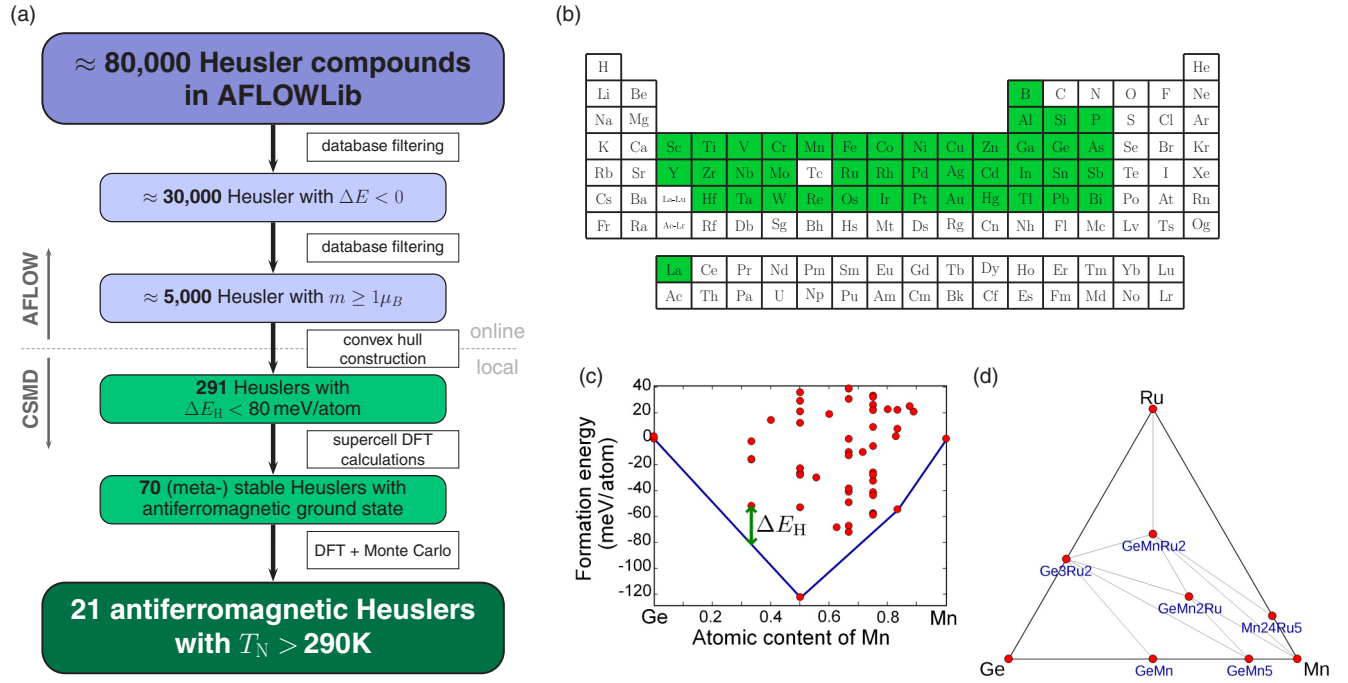

FIG. 1. Overview of the screening method. (a) Complete workflow of the method. The upper part (purple shaded) shows data already present in the AFLOWLib. The lower part (green shaded) reflects the extended calculations done at the Center for Spinelectronic Materials and Devices (CSMD). (b) Green colored elements are included in the screening process. (c) and (d) Examples of zero-temperature phase diagrams. (c) The binary phase diagram of Ge-Mn, the blue line is the convex hull. The green arrow indicates the distance to the convex hull ΔE_{H}. (d) The ternary phase diagram for Ge-Mn-Ru. The corners, edges, and inner area represents elemental, binary, and ternary stoichiometries, respectively. The lines are two-dimensional projections of the faces of the convex hull.

possible antiferromagnetic states are performed to determine the magnetic ground state. Because common spintronic devices operate at room temperature or above, the Néel temperatures are calculated for all candidates that are identified to have an antiferromagnetic ground state. This workflow is sketched in Fig. 1(a).

II. METHODS

As we are aiming to find new materials for spintronic (thin film) applications we define three basic criteria for the database search within the AFLOWLib:

(1) *Suitable elements*—exclude elements which are not suitable for thin film deposition and processing.

(2) *Magnetism*—at least one atom needs to have a nonvanishing magnetic moment.

(3) *Stability*—the material needs to be stable against decomposition.

Besides radioactive elements, we especially excluded elements not suitable for thin film preparation (alkaline metals, noble gases) or that impose significant constraints on the type of deposition technology (halogens, chalcogens). Except for La, lanthanides are not yet included in the ternary phases in the AFLOWLib. The full list of included elements is visualized in a periodic table of the elements in Fig. 1(b). To exclude nonmagnetic materials we restricted our search to compounds, where the sum of the absolute magnetic moments of the atoms in the Heusler material, found in spin decomposition provided by the AFLOWLib database, is at least $1\mu_{\mathrm{B}}$. Furthermore, we restricted the search to a negative formation energy ΔE to ensure thermodynamic stability of the compound. For Heusler compounds X_2YZ the formation energy ΔE is

$$\Delta E(X_2YZ) = E(X_2YZ) - 2E(X) - E(Y) - E(Z), \quad (1)$$

where $E(X)$ is the total energy of the minimum-energy structure of element X. The formation energy as well as the magnetic moment is calculated for every compound in the AFLOWLib and available in the online library [16] including a search engine with corresponding filters.

A. Phase stability

The AFLOWLib contains calculated properties for more than one million ternary phases. Out of these, about 30 000 compounds in the $L2_1$ Heusler structure are potentially stable, i.e., have a negative formation energy $\Delta E < 0$. Additionally, restricting the sum of absolute magnetic moments to $|m| \geqslant 1.0\mu_{\mathrm{B}}$/f.u. yields roughly 5000 compounds. For the compounds only containing the elements shown in Fig. 1(b) we calculated the phase diagrams and the convex hull.

To compute the phase diagrams, we gather the formation energies for every elemental, binary, and ternary phase containing the elements X, Y, and/or Z included in the AFLOWLib using the AFLOWLib API [17]. Plotting the formation energy as a function of the stoichiometry creates the phase diagrams. Within these phase diagrams, we calculated the convex hull, which is the smallest subset of a point set that contains the whole original set. As only phases with a negative formation energy are of interest, only the negative part of the convex hull is relevant here.

Phases with a distance to the convex hull ΔE_H can reduce their total energy by phase decomposition into energetically lower lying phases on the hull. Therefore, ΔE_H is a measure for the phase stability of a certain phase. Phases which are a part of the convex hull, i.e., $\Delta E_H = 0$, are stable against decomposition. We calculate the convex hull using the QHULL tool [18] and the corresponding distance ΔE_H to it.

Exemplarily, a two-dimensional (2D) phase diagram for Ge-Mn is shown in Fig. 1(c). The solid blue line represents the convex hull and the green arrow is the distance to the convex hull ΔE_H, which is a measure for stability. For ternary compounds, the composition is visualized as an equilateral triangle. As these phase diagrams are three dimensional, the hull is usually displayed as a projection into the xy plane. In Fig. 1(d), this is shown for the Ge-Mn-Ru system. The points in the plot represent the stable phases of the Ge-Mn-Ru system.

Each phase diagram consists of roughly 1000 elemental and binary phases and about 30 ternary phases, highly depending on the included elements. Every phase represents a single DFT calculation with full relaxation of internal and unit cell degrees of freedom. In the database, only magnetic configurations with initially parallel magnetic moments are considered. Thus, we need to take into account that the magnetic ground state of any phase may differ from the AFLOWLib data. As a consequence, the actual convex hull could be slightly lowered in some cases. Due to this, experimental thermodynamic stability may differ from the tendency predicted by ΔE_H. A compound which is thermodynamically unstable in its ferromagnetic state could become stable in the antiferromagnetic state. For example, we find energy gains of up to 60 meV/atom from the antiferromagnetic states in the Heusler compounds. To address this for the Heusler compounds we investigated in detail, we define a tolerance of $\Delta E_H < 80$ meV per atom for the evaluation of the phase stability. This approach is further supported by the consideration of materials which are known to be stable in experiments. In the well known case of Cu_2MnAl, the prototype Heusler, we find $\Delta E_H = 63.8$ meV/atom, which is in agreement with the results of other computational materials databases such as the Materials Project [19,20].

B. Ground state determination

Using this tolerance, we identify 291 Heusler compounds that are potentially stable. Out of them, 74 are found directly on the corresponding convex hull, i.e., $\Delta E_H = 0$. For these 291 candidates, explicit ground state calculations for the ferromagnetic (FM) and antiferromagnetic configurations AF1 and AF2 were done. These antiferromagnetic orders are sketched in Fig. 2. Here the gray spheres represent atoms in an fcc lattice and the arrows represent the orientation of their magnetic moments. The shaded areas represent the corresponding alternating planes of parallel magnetic moments. In the AF1 state [Fig. 2(a)], the magnetic moment orientation is staggered in the [001] planes; in the AF2 state [Fig. 2(b)] the magnetic moment orientation is staggered in the [111] planes. Due to the inversion symmetry, all {001} or {111} arrangements are equivalent, respectively. Since spin-orbit coupling is neglected in our calculations, the orientation of the magnetic moments with respect to the lattice plays no role.

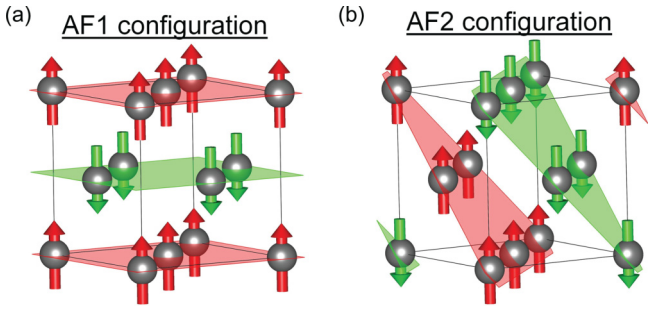

FIG. 2. Sketches of the investigated highly symmetric antiferromagnetic states: (a) AF1 state and (b) AF2 state. The gray spheres represent atoms and the arrows the corresponding magnetic moments. Shaded areas show the planes of parallel moments. Sketches are created with VESTA [21].

The density functional theory calculations presented in this work are done using the Vienna *ab initio* simulation package (VASP) [22,23], which is also used by the AFLOWLib. Within the framework of the projector augmented wave (PAW) method [24], the generalized gradient approximation (GGA) with the Perdew-Burke-Ernzerhof (PBE) [25] exchange-correlation functional is used. The same PAW potentials as in the AFLOWLib calculation are used. Detailed information on parameters and potentials used to generate the AFLOWLib database can be found in Refs. [26,27]. The cutoff for the plane wave expansion is set to 500 eV. The AF1 and AF2 states are calculated with eight-atom supercells that maximize the symmetry for the corresponding configurations.

The numerical parameters are set to achieve a convergence of <1 meV for the total energy, which turns out to be a typical scale for energy differences between FM and AF states. Sampling of the Brillouin zone is done using a Γ-centered $20 \times 20 \times 20$ **k**-point mesh for the FM state. For the AF1 and AF2 state calculations the number of **k** points is adjusted to the size of the corresponding Brillouin zone, such that the density of **k** points remains constant. The convergence with respect to the number of **k** points is tested for each compound comparing the energy to a calculation using fewer **k** points. If the desired precision of 1 meV is not achieved, calculations are repeated with successively denser **k**-point meshes. Magnetic moments in the starting configuration for each atom are set according to Hund's rules. In the supercells, the whole groups of X_2YZ are initially aligned antiparallel. A full structural relaxation is included in every calculation relaxing internal degrees of freedom and the lattice constants.

In addition to checking the thermodynamic stability, covered by the convex hull considerations, we evaluated the elastic stability for selected compounds by calculating the elastic tensor. It is determined using the VASP code by performing finite lattice distortions and deriving elastic constants from the strain-stress relationship [28]. Elastic instability is indicated by negative eigenvalues of the elastic tensor.

C. Néel temperature estimation

The calculations for stable antiferromagnetic ground states are repeated using the Munich spin-polarized relativistic KKR (SPR-KKR) program [29,30]. The full-potential mode is used

to accurately reproduce results from the PAW calculations. The angular momentum cutoff is set to $l_{\max} = 3$ and a dense **k**-point mesh of $20 \times 20 \times 20$ **k** points is used. The integration of the Green's function is done on an arc with 60 energy points in the complex plane. The equilibrium lattice constants and the magnetic moments from the previous calculations are used as the initial configuration.

The SPR-KKR package allows us to map a system onto a classical Heisenberg Hamiltonian given by

$$\mathcal{H} = -\sum_{i \neq j} J_{ij} \mathbf{S}_i \mathbf{S}_j, \tag{2}$$

where $\mathbf{S}_i$ and $\mathbf{S}_j$ are unit vectors of the magnetic moments at site i and j. J_{ij} are the Heisenberg exchange coupling parameters representing the exchange interaction between the magnetic moment at sites i and j. $J_{ij} > 0$ is a ferromagnetic coupling and $J_{ij} < 0$ is an antiferromagnetic coupling. These coupling parameters are determined using the method of Liechtenstein *et al.* [31] on a cluster with a radius of $r = 4.5a$ in real space, where a is the lattice parameter of the cubic unit cell.

With the knowledge of J_{ij}, the Néel temperature for the compound can be estimated in the mean-field approximation by solving a set of coupled equations

$$\frac{3}{2} k_B T_N^{MF} \langle \mathbf{S}_\mu \rangle = \sum_\nu J^0_{\mu\nu} \langle \mathbf{S}_\nu \rangle, \tag{3}$$

with

$$J^0_{\mu\nu} = \sum_{\mathbf{r} \neq 0} J^{\mathbf{r}}_{\mu\nu}, \tag{4}$$

where μ and ν label different sublattices. $J^{\mathbf{r}}_{\mu\nu}$ represents the interaction between sites in sublattices μ and ν separated by **r**. $\langle \mathbf{S}_\mu \rangle$ is the average z component of the unit vector $\mathbf{S}_\mu$ in the sublattice μ. T_N^{MF} is the estimated Néel temperature and k_B is the Boltzmann constant. The largest eigenvalue of the $J^0_{\mu\nu}$ matrix determines the Néel temperature [32,33].

However, the approximated Néel temperature in the mean-field approximation is typically overestimated [34]. To get a more accurate approximation, Monte Carlo (MC) simulations are performed. Previously we have shown that this method yields excellent results [35]. The simulation box in our Monte Carlo calculations consists of $20 \times 20 \times 20$ antiferromagnetic unit cells with periodic boundary conditions. Atoms with vanishing magnetic moments are neglected to reduce the computational load. This results in a total number of 16 000 atoms for the usual two magnetic atoms per antiferromagnetic cell. A total number of 3200 interactions per antiferromagnetic unit cell is included in that case. The simulation uses an implementation of the Metropolis algorithm [36], where at each step a randomly chosen reorientation of one spin is put into trial. To estimate the Néel temperature, simulations are done on a temperature range up to $1.25 \cdot T_N^{MF}$. The temperature step size is set to approximately $1.25 \cdot T_N^{MF}/100$. Each system is initially relaxed by 20 000 MC steps per atom. For each temperature step 2000 MC steps per atom are performed as a prerelaxation using the previous configuration as a starting configuration for the new temperature. The prerelaxation is followed by an integration over 20 000 MC steps per atom.

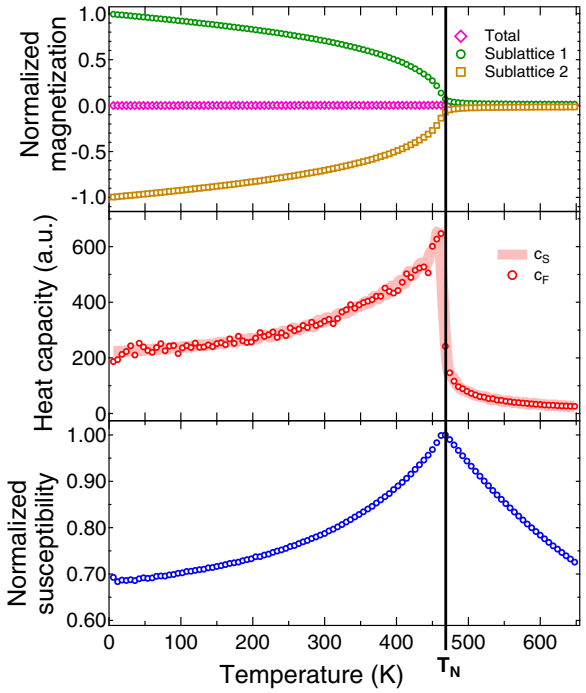

FIG. 3. Determination of the Néel temperature. Temperature dependence of the normalized magnetization (top), heat capacity (middle), and normalized susceptibility (bottom) from a Monte Carlo simulation for Mn_2PtAu in the AF1 state are shown. The solid vertical line indicates the Néel temperature.

Normalized sublattice magnetizations, the heat capacity, and the magnetic susceptibility from a Monte Carlo simulation of the Mn_2PtAu system in the AF1 state are shown in Fig. 3. The heat capacity c_S is obtained as the numerical derivative of the total energy. The heat capacity c_F and the susceptibility χ are obtained from the fluctuation-dissipation theorem by

$$c_F = \frac{1}{k_B T^2} (\langle E^2 \rangle - \langle E \rangle^2), \tag{5}$$

$$\chi = \frac{1}{k_B T} (\langle m^2 \rangle - \langle m \rangle^2), \tag{6}$$

where T is the temperature and k_B is the Boltzmann constant. Both c_F and c_S match precisely. The susceptibility decreases to 2/3 of its maximum for $T \to 0$ as expected for antiferromagnets. The heat capacity shows a divergence at the phase transition. Fitting a cubic spline to the total energy and determining the steepest decay using the second derivative yields the transition temperature most reliably, thus all Néel temperatures are calculated this way.

III. RESULTS

To determine the energetic ground state, we calculated the energy differences to the FM state $\Delta E_{AF1} = E_{AF1} - E_{FM}$ and $\Delta E_{AF2} = E_{AF2} - E_{FM}$ for all candidate materials. Out of the 291 potentially stable compounds, we identify 70 compounds as antiferromagnetic for which we calculate the Heisenberg exchange parameters J_{ij} and Néel temperatures T_N^{MC} using a Monte Carlo simulation. We find 21 Heusler compounds with a Néel temperature above room temperature. These are

TABLE I. Heusler compounds with a predicted Néel T_N^{MC} temperature above room temperature. The table shows the energy difference of the compound to the convex hull ΔE_H and the most stable antiferromagnetic configuration. If the Néel temperature is higher for the less stable AF configuration, it is given in brackets. Experimental Néel temperatures are given where available. Elastically stable compounds are printed in bold.

Compound	T_N^{MC} (K)	ΔE_H (meV/atom)	State	T_N^{expt} (K)
Al_2MnOs	308	72	AF2	–
Au_2CuMn	316	31	AF2	–
Fe_2IrRh	956	54	AF1	–
Fe_2NbGe	310	16	AF1	–
Fe_2NbSn	355	44	AF1	–
Fe_2TaSn	338	68	AF1	–
Hf_2ReV	177 (369)	72	AF2	–
Mn_2NiPd	819	71	AF1	–
Mn_2PdAu	385 (520)	40	AF1	–
Mn_2PdPt	442	0	AF1	345 [37]
Mn_2PdRh	192 (873)	6	AF2	–
Mn_2PtAu	462 (495)	35	AF1	–
Mn_2PtCu	373	53	AF1	–
Os_2MnSi	396	18	AF2	–
Pd_2AuCr	225 (747)	65	AF2	–
Pd_2CrCu	166 (408)	61	AF2	–
Ru_2FeGa	308	2	AF2	[a][39]
Ru_2HfMn	409	77	AF2	–
Ru_2MnGe	307	0	AF2	353 [40]
Ru_2MnSi	365	0	AF2	313 [41]
Ru_2TiMn	348	51	AF2	–

[a]Antiferromagnetism predicted.

summarized together with their distance to the convex hull ΔE_H (as a measure for stability) and the lowest-energy AF state in Table I. Experimentally measured Néel temperatures are only available for four of the 21 compounds; they are within a 25% error margin in agreement with our calculation. Notably, the AF2 state is found more often than the AF1 state. However, the highest Néel temperature is found for the AF1 state in Fe_2IrRh (956 K). Unfortunately it turns out that the majority of the Heusler compounds with high Néel temperature have a fairly large distance from the convex hull. It has to be left to experiment to assess the stability of these phases in both bulk as well as thin film forms.

In Table II we summarize the most stable antiferromagnetic Heuslers with distance to the convex hull $\Delta E_H = 0$. Only three compounds, Mn_2PdPt, Ru_2MnGe, and Ru_2MnSi, are predicted to have Néel temperatures above room temperature. These are already known experimentally. The result of our investigation predicting Mn_2PdPt as a stable antiferromagnetic Heusler compound has been confirmed by experiments very recently [37]. Furthermore, Ru-based compounds make up half of the compounds that are stable according to our analysis. About half of the predicted compounds were already investigated experimentally and to the best of our knowledge the experiments confirm our predictions. The experimental Néel temperatures resemble the predicted ones well, except for the Ir-based compounds.

TABLE II. The most stable antiferromagnetic Heusler compounds with $\Delta E_H = 0$ meV. The corresponding Néel temperatures of the most stable antiferromagnetic state are shown. If the Néel temperature is higher for the less stable AF configuration, it is given in brackets. Experimental Néel temperatures are given where available. Compounds synthesized in experiments, but not yet investigated magnetically are marked with *stable*. Elastically stable compounds are printed in bold.

Compound	T_N^{MC} (K)	State	T_N^{expt} (K)
Fe_2VGe	252	AF1	–
Ir_2MnAl	192	AF2	500 [42]
Ir_2MnGa	190	AF2	65 [43]
Mn_2PdPt	442	AF1	345 [37]
Mn_2PtRh	189	AF2	–
Pd_2AuMn	177	AF1	–
Pd_2CuMn	244	AF1	–
Rh_2MnGa	163	AF2	stable [44]
Rh_2MnIn	103	AF2	stable [44]
Ru_2CrAl	83	AF1	–
Ru_2CrGa	98	AF1	–
Ru_2CrGe	37	AF2	13 (AF2) [45]
Ru_2CrSi	41	AF2	14 [46]
Ru_2MnAl	37 (50)	AF2	stable [47]
Ru_2MnGe	307	AF2	353 [40]
Ru_2MnSi	365	AF2	313 [41]
Ru_2VGe	75	AF1	paramagnetic [48]
Ru_2VSi	69	AF1	stable [47]

For the most promising candidates summarized in Tables I and II we evaluated the elastical stability by calculating the elastic tensor. If the elastic tensor is positive definite, the material is considered as elastically stable and printed in bold in the tables. This is found for all compounds, where experimental data are already available except Mn_2PdPt. Interestingly, albeit predicted elastically unstable, Mn_2PdPt has been synthesized recently by arc melting [37]. This could be indicative of an antiferromagnetic ground state different from AF1 stabilizing the structure. Furthermore, except Fe_2VGe and Pd_2AuMn all compounds with $\Delta E_H = 0$ are predicted to be elastically stable. For compounds with large Néel temperatures we find about half of the compounds to be elastically unstable. This is reflected by the thermodynamic stability, where most of them have a $\Delta E_H > 0$. Generally, however, neither thermodynamic stability includes elastical stability, nor vice versa.

The Néel temperatures as well as detailed structural and magnetic information for all antiferromagnetic Heusler compounds can be found in the Supplemental Material [38]. In general, the calculated Néel temperatures cover a wide range from nearly 0 to 956 K. The highest temperature for the AF1 state is obtained for Fe_2IrRh at 956 K and in the AF2 state it is 520 K for Mn_2PdAu. However, our investigation of elastical stability predicts these compounds to be unstable. The elastically stable compounds with the highest Néel temperatures are Fe_2NbSn (355 K) in the AF1 state and Ru_2HfMn (409 K) in the AF2 state. Our predictions of the magnetic ground states are confirmed by experiments: for ten

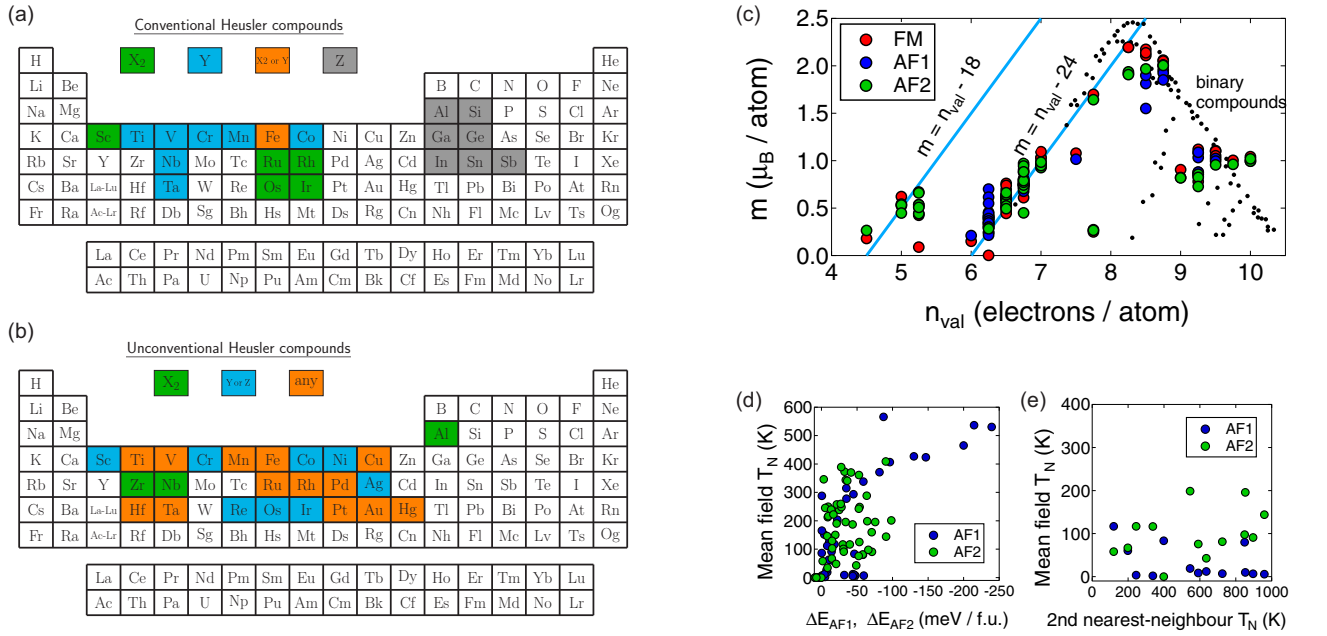

FIG. 4. Results of the screening. (a) Distribution of elements for conventional Heusler compounds (Z = main group element). (b) Same visualization for unconventional Heusler compounds. (c) Magnetic moments of the investigated Heusler compounds plotted versus the number of valence electrons. A Slater-Pauling-like behaviour (blue lines) is found. Black dots are data for binary phases adopted from Ref. [52]. (d) Calculated Néel temperature from the mean-field approximation plotted against the corresponding energy gain ΔE_{AF1} and ΔE_{AF2}. No direct relation is found, indicating the importance of long range interactions. (e) For Heusler compounds found to be stable in both AF1 and AF2, a Néel temperature estimation from a second nearest-neighbor model and a mean-field approach plotted against each other. Here no relation is found as well, supporting the importance of long range interactions not covered by a simple second nearest-neighbor model.

of the compounds, antiferromagnetic phases were experimentally confirmed in agreement with the predictions; a neutron diffraction analysis of Ru_2CrGe identified an AF2 state, in agreement with our prediction. Four additional compounds we predict to be antiferromagnetic already have been investigated experimentally and found to be stable, however, no magnetic measurements were published yet. For another one, Ru_2FeGa, antiferromagnetism was already predicted [39], but not yet experimentally confirmed.

There are four compounds that require additional discussion: experimentally, Fe_2CrSi and Fe_2TiSb are found to be unstable [49,50], Ru_2CrSn shows a spinglass behavior [45], and Ru_2VGe is found to be paramagnetic [48]. For Fe-Ti-Sb, a disordered, more stable phase ($Fe_{1.5}TiSb$ [49]) not included in the AFLOWLib exists. For Fe_2CrSi the distance to the convex hull $\Delta E_{\mathrm{H}} = 76.1$ meV/atom is quite high (but still within our tolerance), which means it is very likely that this compound is unstable in the experiment. For Ru_2VGe we have to consider that our calculations (as well as the AFLOWLib calculations) are based on the Perdew-Burke-Ernzerhof generalized gradient approximation, which systematically overestimates the lattice constants of most solids [51] due to too strong exchange energy. For compounds on the verge between ferro- and paramagnetism, the enlarged lattice constant and enhanced exchange interaction may give rise to a nonzero ordering temperature contrary to the experiment. As we consider only two highly symmetric antiferromagnetic states (AF1 and AF2), we are not able to correctly identify more complex states such as spin spirals or glassy states.

The Néel temperatures of already known antiferromagnetic Heuslers are significantly different from our prediction in some cases. Typically, the experimental Néel temperatures are lower than the predicted ones, with the exception of Ir_2MnAl, which has a significantly higher Néel temperature in the experiment. Still, the computed transition temperatures give an indication if the material would be antiferromagnetic around room temperature or not.

We demonstrate that the high-throughput approach to materials discovery can be applied to the search for novel antiferromagnetic materials, which we exemplify by screening the Heusler compounds for antiferromagnetic ground states. To the best of our knowledge, there are no ordered Heusler compounds with an antiferromagnetic ground state reported in the literature that we do not correctly identify in our calculations; in other words, we find no cases of false negative errors. Also, we do not erroneously assign antiferromagnetic ground states to compounds that are known to be ferromagnetic instead, so we also find no false positive errors. Thus, the prediction of new antiferromagnetic materials based on a combinatorial screening of the AFLOWLib works with very good selectivity.

Now we investigate the distribution of elements among the conventional Heusler compounds, i.e., Heusler compounds X_2YZ where Z is a main group element, and for unconventional Heusler compounds where Z is a transition metal. The preference of the elements to occupy the different sites is shown in Figs. 4(a) and 4(b). For the conventional Heusler compounds [Fig. 4(a)], a clear tendency can be seen: the X_2 position is taken by the platinum group metals Ru, Rh, Os,

and Ir and Sc. Among the other transition metals, only Fe is found on the Y position in a few cases. In contrast, for the unconventional Heusler compounds, no clear tendencies for the elements to occupy specific atomic positions are found as shown in Fig. 4(b).

The largest (negative) energy difference is $\Delta E_{\mathrm{AF1}} = -239$ meV/f.u. for Mn_2PtAu in the AF1 state. No correlation between the energy differences ΔE_{AF1} and ΔE_{AF2} can be found. The equilibrium lattice constants typically differ from the ferromagnetic state in a subpermille range. In the AF1 state, Fe_2YZ and Mn_2YZ compounds tend to distort tetragonally, increasing the lattice constant by a few percent in the [001] direction due to the magnetic moment localized on the X_2 atoms. The unit cell volume remains approximately the same in these cases. The majority of compounds carries the magnetic moment exclusively on the Y or Z atom, except for the Fe_2YZ and Mn_2YZ compounds. For the absolute magnetic moment $m_{\mathrm{abs}} = \sum_i |m_i|$ per atom we find a Slater-Pauling-like behavior, as can be seen by plotting m_{abs} as a function of the number of valence electrons n_{val} per atom in Fig. 4(c). All three configurations FM (red), AF1 (blue), and AF2 (green) are shown. Here we find many compounds that approximately follow the well-known Slater-Pauling rule (blue lines) $m = n_{\mathrm{val}} - 24$ for Heusler compounds. Furthermore, some of the compounds seem to follow the $m = n_{\mathrm{val}} - 18$ rule for the half Heusler structure [52].

Based on the results obtained from the full real-space J_{ij} calculation, Néel temperatures $T_{\mathrm{N}}^{\mathrm{MF}}$ were estimated by a mean-field approximation (see Methods). The usual trend of $T_{\mathrm{N}}^{\mathrm{MF}} > T_{\mathrm{N}}^{\mathrm{MC}}$ is found. In Fig. 4(d) we compare the resulting $T_{\mathrm{N}}^{\mathrm{MF}}$ with the energy gain in the antiferromagnetic configurations ΔE_{AF1} and ΔE_{AF2}. A weak correlation between the energy gain and the Néel temperature is evident, although there are many examples that have small energy gain but still large Néel temperature. The highest values for energy gains are obtained for Fe_2YZ and Mn_2YZ compounds in AF1 configurations, where the lattice distortion increases the energy difference and stabilizes the antiferromagnetism. A further investigation is done in a simple second nearest-neighbor model. For compounds of the X_2YZ type where only Y has a magnetic moment, the first and second neighbor exchange interactions can be written as

$$\begin{aligned} \Delta E_{\mathrm{AF1}} &= 8J_1, \\ \Delta E_{\mathrm{AF2}} &= 6J_1 + 6J_2. \end{aligned} \tag{7}$$

In the mean-field approximation, one can now write the Néel temperature as $\frac{3}{2}k_{\mathrm{B}}T_{\mathrm{N}}^{\mathrm{2nn}} = |12J_1 + 6J_2| = |\frac{3}{4}\Delta E_{\mathrm{AF1}} + \Delta E_{\mathrm{AF2}}|$. In Fig. 4(e) we compare the values of $T_{\mathrm{N}}^{\mathrm{MF}}$ from the calculation with the values of $T_{\mathrm{N}}^{\mathrm{2nn}}$ for 13 compounds that gain energy with respect to the FM state in both AF configurations. It turns out that the second-nearest neighbor model greatly overestimates the Néel temperature in most cases and no clear correlation between the two Néel temperature estimates is observed. These results indicate that interactions at much longer range play a significant role in determining the transition temperature. Thus, especially the second nearest-neighbor approach is insufficient here; a detailed evaluation taking long range interactions into account is thus mandatory and is the basis for our Monte Carlo estimates of the Néel temperatures given in Tables I and II.

IV. CONCLUSION

In conclusion, we identify 70 antiferromagnetic Heusler compounds that are expected to be stable or metastable in experiments. Comparison with available experimental data shows that our high-throughput approach has excellent selectivity. Similar results are found by Sanvito and co-workers in a recent publication reporting on the same method [37], however, focusing on ferromagnetic Heusler compounds. Especially, in one of their exemplary experiments they found one of the predicted compounds (Mn_2PdPt) to be antiferromagnetic, where the experimental results are in good agreement with our predictions. We identify 21 compounds to have a Néel temperature above room temperature, making them candidates for spintronic applications. In order to guide experimentalists and in addition to the thermodynamic stability, we investigated the elastical stability for the most promising materials. Within our framework the compounds Al_2MnOs, Fe_2NbSn, Fe_2TaSn, Hf_2ReV, Mn_2PdRh, Os_2MnSi, Ru_2FeGa, Ru_2HfMn, and Ru_2TiMn are predicted as novel antiferromagnets with thermodynamic and elastical stability as well as a high Néel temperature.

However, the systematic approach we are using is limited by several aspects. Besides the main limitation due to available computational power, the accuracy of the convex hull calculations strongly depends on the number of phases used in the calculation. There may exist more binary and especially ternary phases not considered in the calculations, rendering a compound stable which actually is not. Furthermore, to allow for some tolerance in the convex hull calculation to include phases that are known to be stable by experiment, we introduced a cutoff for the distance to the convex hull ΔE_{H}. Compounds with $\Delta E_{\mathrm{H}} < 80$ meV per atom are considered potentially stable, although they might not be, as is the case for Fe_2CrSi. Also, atomic disorder was neglected. Atoms in the Heusler structure may mix, e.g., between Y and Z sites, leading to a reduction in order, which can seriously affect the magnetic properties. For example, the B2 ordered compound Ni_2MnAl is antiferromagnetic, although the $L2_1$ ordered phase is ferromagnetic [53]. The Néel temperature can also be affected by the degree of order in the compound [54]. Within our calculations we only included two collinear antiferromagnetic states, AF1 and AF2. However, there is in principle an infinite number of possible antiferromagnetic arrangements. More complex ground states including noncollinear spin spiral or frustrated states are yet to be investigated. Despite these possible shortcomings, we claim to have identified essentially all possible, fully ordered antiferromagnetic Heusler compounds with either AF1 or AF2 ground state, that are suitable for applications in spintronic devices.

ACKNOWLEDGMENT

The research leading to these results has received funding from the European Union Seventh Framework Programme (FP7/2007-2013) under Grant Agreement No. NMP3-SL-2013-604398 (HARFIR).

[1] M. N. Baibich, J. M. Broto, A. Fert, F. Nguyen Van Dau, F. Petroff, P. Etienne, G. Creuzet, A. Friederich, and J. Chazelas, Phys. Rev. Lett. **61**, 2472 (1988).

[2] G. Binasch, P. Grünberg, F. Saurenbach, and W. Zinn, Phys. Rev. B **39**, 4828 (1989).

[3] J. F. Gregg, I. Petej, E. Jouguelet, and C. Dennis, J. Phys. D: Appl. Phys. **35**, R121 (2002).

[4] C. Chappert, A. Fert, and F. N. Van Dau, Nat. Mater. **6**, 813 (2007).

[5] A. V. Khvalkovskiy *et al.*, J. Phys. D: Appl. Phys. **46**, 074001 (2013).

[6] J. C. Slonczewski, J. Magn. Magn. Mater. **159**, L1 (1996).

[7] L. Berger, Phys. Rev. B **54**, 9353 (1996).

[8] J. Nogués and I. K. Schuller, J. Magn. Magn. Mater. **192**, 203 (1999).

[9] A. E. Berkowitz and K. Takano, J. Magn. Magn. Mater. **200**, 552 (1999).

[10] T. Jungwirth, X. Marti, P. Wadley, and J. Wunderlich, Nat. Nanotechnol. **11**, 231 (2016).

[11] P. Wadley *et al.*, Science **351**, 587 (2016).

[12] A. Kohn *et al.*, Sci. Rep. **3**, 2412 (2013).

[13] WebElements Periodic Table (2015), www.webelements.com

[14] M. Meinert, B. Büker, D. Graulich, and M. Dunz, Phys. Rev. B **92**, 144408 (2015).

[15] S. Curtarolo *et al.*, Comput. Mater. Sci. **58**, 227 (2012).

[16] AFLOW distributed materials property repository (2016), www.aflowlib.org

[17] R. H. Taylor *et al.*, Comput. Mater. Sci. **93**, 178 (2014).

[18] C. B. Barber, D. P. Dobkin, and H. Huhdanpaa, ACM Trans. Math. Soft. **22**, 469 (1996).

[19] The Materials Project (2017), www.materialsproject.org

[20] A. Jain *et al.*, APL Mater. **1**, 011002 (2013).

[21] K. Momma and F. Izumi, J. Appl. Crystallogr. **44**, 1272 (2011).

[22] G. Kresse and J. Furthmüller, Phys. Rev. B **54**, 11169 (1996).

[23] G. Kresse and D. Joubert, Phys. Rev. B **59**, 1758 (1999).

[24] P. E. Blöchl, Phys. Rev. B **50**, 17953 (1994).

[25] J. P. Perdew, K. Burke, and M. Ernzerhof, Phys. Rev. Lett. **77**, 3865 (1996).

[26] S. Curtarolo *et al.*, Comput. Mater. Sci. **58**, 218 (2012).

[27] C. E. Calderon *et al.*, Comput. Mater. Sci. **108**, 233 (2015).

[28] Y. Le Page and P. Saxe, Phys. Rev. B **65**, 104104 (2002).

[29] H. Ebert *et al.*, The Munich SPR-KKR package, version 5.4, http://ebert.cup.uni-muenchen.de/SPRKKR

[30] H. Ebert, D. Ködderitzsch, and J. Minár, Rep. Prog. Phys. **74**, 096501 (2011).

[31] A. I. Liechtenstein, M. I. Katsnelson, V. P. Antropov, and V. A. Gubanov, J. Magn. Magn. Mater. **67**, 65 (1987).

[32] P. W. Anderson, *Solid State Physics*, edited by F. Seitz and D. Turnbull (Academic, New York, 1963), Vol. 14, pp. 99–214.

[33] E. Şaşioğlu, L. M. Sandratskii, and P. Bruno, J. Phys.: Condens. Matter **17**, 995 (2005).

[34] D. A. Garanin, Phys. Rev. B **53**, 11593 (1996).

[35] M. Meinert, J. Phys.: Condens. Matter **28**, 056006 (2016).

[36] N. Metropolis, A. W. Rosenbluth, M. N. Rosenbluth, A. H. Teller, and E. Teller, J. Chem. Phys. **21**, 1087 (1953).

[37] S. Sanvito *et al.*, Sci. Adv. **3**, e1602241 (2017).

[38] See Supplemental Material at http://link.aps.org/supplemental/10.1103/PhysRevMaterials.1.034404 for detailed structural and magnetic properties of all predicted antiferromagnetic compounds.

[39] S. N. Mishra *et al.*, Hyperfine Interact. **34**, 519 (1987).

[40] N. Fukatani, K. Inagaki, T. Miyawaki, K. Ueda, and H. Asano, J. Appl. Phys. **113**, 17C103 (2013).

[41] T. Kanomata, M. Kikuchi, and H. Yamauchi, J. Alloys Compd. **414**, 1 (2006).

[42] H. Masumoto and K. Watanabe, J. Phys. Soc. Jpn. **32**, 281 (1972).

[43] K. Yoshimura, M. Yamada, M. Mekata, T. Shimizu, and H. Yasuoka, J. Phys. Soc. Jpn. **57**, 409 (1988).

[44] M. Yin and P. Nash, J. Alloys Compd. **650**, 925 (2015).

[45] H. Okada *et al.*, Appl. Phys. Lett. **92**, 062502 (2008).

[46] M. Hiroi *et al.*, J. Korean Phys. Soc. **62**, 2068 (2013).

[47] M. Yin and P. Nash, J. Alloys Compd. **634**, 70 (2015).

[48] S. Mizusaki *et al.*, J. Phys. Conf. Ser. **200**, 052017 (2010).

[49] N. Naghibolashrafi, S. Keshavarz, V. I. Hegde, A. Gupta, W. H. Butler, J. Romero, K. Munira, P. LeClair, D. Mazumdar, J. Ma, A. W. Ghosh, and C. Wolverton, Phys. Rev. B **93**, 104424 (2016).

[50] M. Meinert, T. Hübner, J. Schmalhorst, G. Reiss, and E. Arenholz, J. Appl. Phys. **114**, 113908 (2013).

[51] P. Haas, F. Tran, and P. Blaha, Phys. Rev. B **79**, 085104 (2009).

[52] B. Balke, S. Wurmehl, G. H. Fecher, C. Felser, and J. Kübler, Sci. Technol. Adv. Mater. **9**, 014102 (2008).

[53] E. Simon, J. G. Vida, S. Khmelevskyi, and L. Szunyogh, Phys. Rev. B **92**, 054438 (2015).

[54] S. Khmelevskyi, E. Simon, and L. Szunyogh, Phys. Rev. B **91**, 094432 (2015).